Modelling failures in existing reinforced concrete columns

Kenneth J. Elwood

Abstract: Experimental research and post-earthquake reconnaissance have demonstrated that reinforced concrete columns with light or widely spaced transverse reinforcement are vulnerable to shear failure, and in turn, axial failure during earthquakes. Based on experimental data, failure surfaces have been used to define the onset of shear and axial failure for such columns. After the response of the column intersects the failure surface, the shear or axial strength of the column begins to degrade. This paper introduces a uniaxial material model that incorporates the failure surfaces and the subsequent strength degradation. When used in series with a beam-column element, the uniaxial material model can adequately capture the response of reinforced concrete columns during shear and axial load failure. The performance of the analytical model is compared with results from shake table tests.

Key words: shear failure, axial failure, beam-column elements, failure surface, earthquakes, reinforced concrete, columns, collapse, structural analysis.

Résumé : La recherche expérimentale et la reconnaissance post-séisme ont démontré que les poteaux en béton armé avec une armature transversale légère ou largement espacée sont vulnérables à la rupture par cisaillement et, par après, à la rupture axiale durant les séismes. En s'appuyant sur les données expérimentales, nous avons utilisé les surfaces de rupture pour définir le début de la rupture par cisaillement et axiale pour de tels poteaux. Une fois que la réaction du poteau recoupe la surface de rupture, la résistance au cisaillement ou axiale du poteau commence à se dégrader. Cet article présente un modèle matériel uniaxial qui incorpore les surfaces de rupture et la dégradation subséquente de la résistance. Lorsqu'il est utilisé en série avec un assemblage poteau-poutre, le modèle matériel uniaxial peut capter adéquatement la réponse des poteaux en béton armé durant la rupture par cisaillement et axiale. Le rendement du modèle analytique est comparé aux résultats des essais sur table de vibration.

Mots clés : rupture en cisaillement, rupture axiale, assemblages poteau-poutre, surface de rupture, séismes, béton armé, colonnes, effondrement, calcul des structures.

[Traduit par la Rédaction]

Introduction

Analytical models capable of representing the different failure modes of structural components are required to evaluate the response of a structure as it approaches the collapse limit state. For the evaluation of existing reinforced concrete buildings subjected to earthquake ground motion, there exists a need for analytical models incorporating the initiation of column shear and axial load failures, in addition to the subsequent strength degradation. Given such a model, an engineer could evaluate the influence of column shear and axial load failures on the response of the building frame system. This paper will describe how drift capacity models for shear and axial load failure can be incorporated in an analytical model to detect and initiate strength degradation of column elements.

Several capacity models, or limit state surfaces, have been developed to define the onset of shear failure for reinforced concrete columns. One such model introduced by Elwood and Moehle (2005) relates the shear demand to the drift at shear failure based on the transverse reinforcement and axial load ratios. Based on 50 laboratory tests on reinforced concrete columns yielding in flexure prior to shear failure, the model defines the drift at shear failure as the drift at which the shear capacity has degraded to 80% of the maximum measured shear. As shown in Fig. 1, the point of shear failure, according to the model, is determined by the intersection of an idealized bilinear load–deformation curve for the column and the limit surface defined by the drift capacity model. While it is known that the shear strength will degrade after failure, the shape of the load–deformation curve after intersection with the limit surface is not well understood. Analytical models allowing for a user-defined degrading slope after failure will enable the investigation of the influence of the rate of shear strength degradation on the behaviour of the structural system.

Experimental research has shown that axial failure of a shear-damaged column due to sliding along inclined shear cracks is related to several variables including the axial stress

Received 28 August 2003. Revision accepted 26 April 2004. Published on the NRC Research Press Web site at http://cjce.nrc.ca on 19 October 2004.

K.J. Elwood. Department of Civil Engineering, The University of British Columbia, 6250 Applied Science Lane, Vancouver, BC V6T 1Z4, Canada (e-mail: elwood@civil.ubc.ca).

Written discussion of this article is welcomed and will be received by the Editor until 28 February 2005.

Fig. 1. Shear failure model.

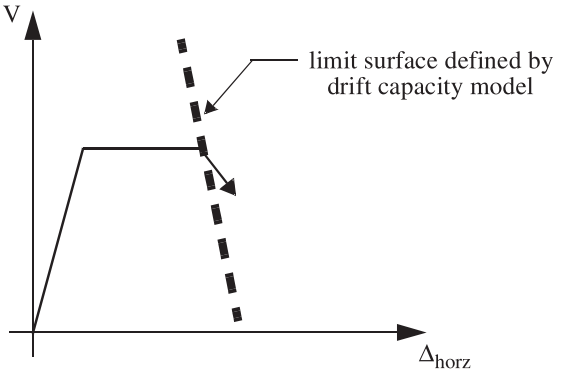

Fig. 2. Axial failure model.

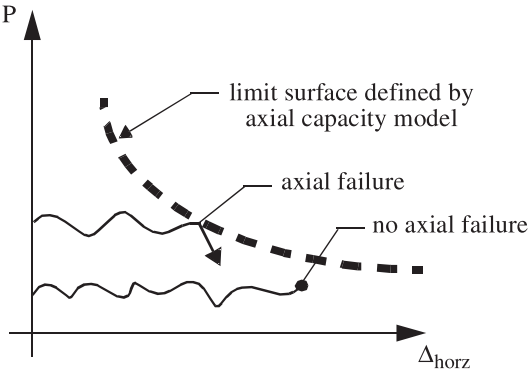

on the column, the amount of transverse reinforcement, and the drift demand. Based on these observations, the onset of axial failure has been described using a shear-friction model (Elwood and Moehle 2003). Similar to the shear failure model described above, this capacity model defines a limit surface at which axial failure is expected to occur, as shown in Fig. 2. According to this model, columns with a low axial load or drift demand would not be expected to experience axial failure. As with the shear failure model, column behaviour after the onset of axial failure is not well understood; however, it is reasonable to expect the axial load – horizontal deflection relation for the damaged column will remain on or below the limit surface after failure is detected.

While describing different phenomenon, the shear and axial capacity models described above both take on the same general form. Both models define a limit surface and trigger a change in the hysteretic behaviour once the appropriate load–deformation relation for the column intersects the limit surface. This similarity allows both capacity models to be implemented in one general material model for structural analysis. Capacity models are frequently used to determine if components have experienced failure by comparing the predicted capacities with demands estimated from an analytical model. Currently this can only be done through post-processing of the results. By implementing this general material model in a finite-element analysis platform, it is possible to capture both the point at which failure is initiated *and* the response of the column after shear and axial load failure during the analysis of the structure. Such a model enables the analysis of structural systems with multiple columns vulnerable to shear and axial load failure as the structural system approaches the collapse limit state.

This paper will describe the general material model proposed above as implemented in the Open System for Earthquake Engineering Simulation (OpenSees), a finite-element analysis platform designed for earthquake engineering simulation (McKenna et al. 2004). First, the concept of material models, as they are applied in OpenSees, will be introduced. Then, in an effort to improve on available shear-critical column models, the new material model described above will be developed. The application of the material model to shear and axial load failure of reinforced concrete columns will be discussed. Finally, the response of the analytical models will be compared with results from shake table tests by Elwood and Moehle (2003).

Uniaxial material models

Uniaxial material models define a constitutive relationship. Depending on the application, the material model could define a relation between stress and strain, force and displacement, moment and curvature, moment and rotation, etc. Uniaxial material models are the lowest level of objects that compose elements in OpenSees. One-dimensional elements, such as springs and truss members, require only one uniaxial material model to define their response. For the zero-length spring element used in this study, the uniaxial material model defines the force–displacement relationship directly.

The uniaxial material model developed in this paper is based on the hysteretic uniaxial material model available in OpenSees. The hysteretic material model has a predefined trilinear backbone and five parameters to define the hysteretic behaviour, including pinching and stiffness degradation. The backbone can include strength degradation, a necessary feature for modelling the behaviour of shear-critical columns. A more detailed description of the hysteretic material model can be found in McKenna et al. (2004).

A shear-critical column model

To motivate the development of a new uniaxial material model, the example of a shear spring in series with a beam-column element, as shown in Fig. 3, is considered for modelling the shear strength degradation of shear-critical columns. The hysteretic uniaxial material model, with strength degradation, can be used to define the constitutive relationship for the shear spring. Any beam-column element capable of modelling the flexural deformations can be used. For the following discussion it will be assumed that the flexural deformations modelled by the beam-column element include both the deformations due to curvatures over the column height and those due to concentrated rotations at the column ends resulting from anchorage bar slip. It should be recognized that the series model shown in Fig. 3 simulates the shear response in an average sense over the height of the column. Intended for the global analysis of a building frame system, this model does not attempt to account for localized deformations over the height of the column.

Similar models have been proposed previously for modelling the post-peak behaviour of existing reinforced concrete

Fig. 3. Shear spring in series model using hysteretic material model.

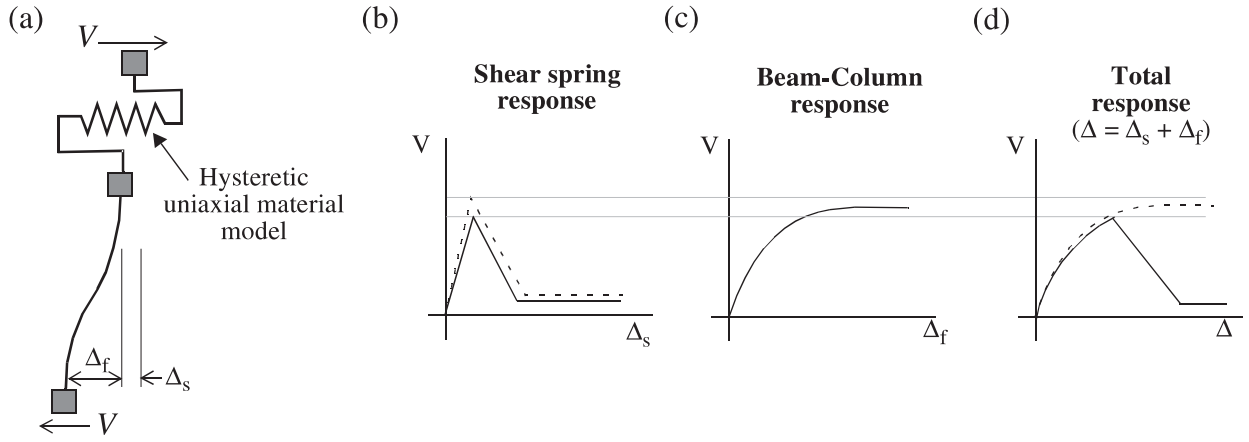

columns (Pincheira et al. 1999; Shirai et al. 2001). In such a model, all the flexural deformations are concentrated in the beam-column element and the shear deformations are modelled by the shear spring. If the shear strength (that is, the peak in the shear spring response backbone) is less than the flexural yield strength of the column (that is, shear corresponding to the development of plastic hinges at the column ends), then the model will be able to capture the degrading shear behaviour, as shown by the solid line for the total response of the column in Fig. 3*d*. If, however, the shear strength is estimated to be higher than the flexural yield strength of the column, then, given limited strain hardening in the flexural response, the model will not capture any shear degradation, as shown by the broken line for the total response of the column in Fig. 3*d*. Several studies have shown, however, that the shear strength decays with increased inelastic deformation (Watanabe and Ichinose 1992; Aschheim and Moehle 1992; Priestley et al. 1994; Sezen 2002). Hence, the total response behaviour depicted by the broken curve in Fig. 3*d* is not realistic for columns that yield in flexure close to their estimated shear strength. The point of shear failure (that is, the start of the degrading behaviour in the total response backbone) should be determined by considering both force and deformation. The model in Fig. 3*a* determines the point of shear failure based only on the column shear.

The behaviour of the series model can be improved by using a uniaxial material model for the shear spring that will only degrade after shear failure has been detected. The detection of shear failure should be based on both the column shear and the total deformation of the column. Calculation of the total deformation requires a coupling of the shear spring and beam-column element. This can be achieved by a new uniaxial material model, entitled limit state material, that traces the behaviour of the beam-column element and changes the backbone of the material model to include strength degradation once the response of the beam-column element exceeds a predefined limit state surface as described in the next section.

Limit state uniaxial material model

The limit state uniaxial material model was developed based on the existing hysteretic material model in OpenSees. The limit state surface used by the uniaxial material model is referred to as a "limit curve" because it is defined in only two dimensions. The choice of these two dimensions, or the ordinate and abscissa on which the limit curve is defined, depends on the application. Three limit curves have been implemented in OpenSees: one to define shear failure (Fig. 1), another to define axial failure (Fig. 2), and a trilinear general purpose limit curve that can be used to approximate any capacity model defining the failure criteria for an element. As shown in Figs. l and 2, the shear force is used for the ordinate of the shear failure limit curve and the axial force is used for the ordinate of the axial failure limit curve. The abscissa is assumed to be a deformation measure, such as interstory drift. Further details on how the limit state material model was implemented in OpenSees can be found elsewhere (Elwood and Moehle 2003).

Prior to failure, the limit state material model follows the same hysteretic rules as defined for the hysteretic material model. The corner points for the pre-failure backbone can be defined such that the response of the uniaxial material model remains linear or is allowed to yield. After each converged step the uniaxial material model queries the beam-column element for its force and deformation and then checks to see if the response has exceeded the selected limit curve. If the limit curve has not been exceeded, then the analysis continues to the next step without any change to the backbone. If the limit curve has been exceeded, then the backbone is redefined to include the degrading slope, K_{deg}, and residual strength, F_{res}. Figure 4 illustrates how the backbone for the force–deformation relation of the limit state material model is redefined upon failure. Exceedance of the limit curve is checked only after each converged load step to avoid "flip-flopping" between the pre- and post-failure states within a single load step. Consequently, small load steps (or time steps for dynamic analysis) are required to accurately determine when the limit curve is exceeded.

Applications of limit state material model

Two examples of how the limit state material model can be used will be presented in the following sections. The first example demonstrates how the uniaxial material model can be used to model column shear failures, while the second demonstrates its application to column axial failures. When

Fig. 4. Redefinition of backbone after failure is detected.

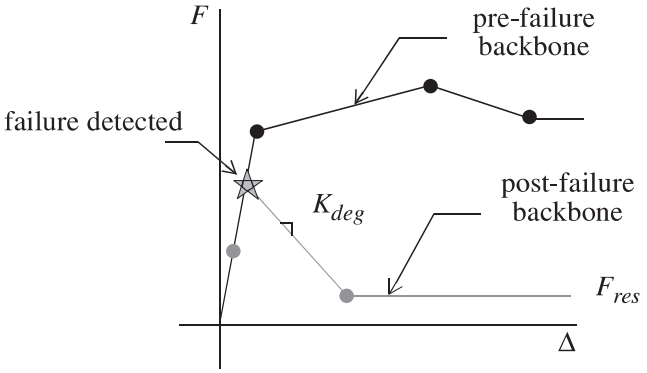

used to model axial failure, the limit state material model incorporates coupling between shear and axial load after failure is detected.

In addition to the examples presented here, the limit state material model can be used to model any failure mode that triggers a sudden change in behaviour for a component. Kang and Wallace (2004) have used the limit state material model to capture the punching shear failure of flat plate slabs. Other examples include the shear failure of reinforced concrete beams, the fracture of welded steel moment connections, and the sliding shear failure of masonry walls. Each failure mode must be defined by a limit curve (capacity model) and the backbone response after failure is detected must be reasonably approximated by a linear degradation in strength, down to a preselected residual value.

Modelling column shear failures

In this example the limit state material model is used to define the force–deformation relationship of a shear spring in series with a beam-column element. The uniaxial material model monitors the response of the beam-column element to detect the onset of shear failure. As shown in Fig. 5, the limit curve is defined based on the column shear, V, and the total displacement, Δ (or the interstory drift, Δ/L). If the column is vulnerable to shear failure *after* flexural yielding, then the drift capacity model proposed by Elwood and Moehle (2005) can be used to define the limit curve

$$[1] \qquad \frac{\Delta_s}{L} = \frac{3}{100} + 4\rho'' - \frac{1}{40}\frac{v}{\sqrt{f'_c}} - \frac{1}{40}\frac{P}{A_g f'_c} \geq \frac{1}{100}$$

where Δ_s/L is the drift ratio at shear failure, ρ'' is the transverse reinforcement ratio, ν is the nominal shear stress (in megapascals), f'_c is the concrete compressive strength (in megapascals), P is the axial load on the column, and A_g is the gross cross-sectional area.

A similar model for shear-critical bridge columns was developed by Ricles et al. (1998) by incorporating the shear strength model by Priestley et al. (1994) to initiate shear failure. However, as shown in Elwood and Moehle (2005), the use of a shear strength model to predict the point at which shear failure occurs can result in an unacceptably large variability in the predicted drift at shear failure for shear-critical building columns.

The pre-failure backbone for the limit state material model is selected as linear with a steep slope equal to the shear stiffness of an uncracked column. Note that by defining the limit curve based on the total displacement, the shear deformations are included in the displacements monitored by the uniaxial material model, and shear failure is based on the sum of the flexure and shear deformations.

When the beam-column response reaches the limit curve for the first time, the backbone of the shear spring is redefined, as shown in Fig. 4, to include the degrading slope, K_{deg}, and residual strength, F_{res}. Since shear failure will influence the strength of the column in both directions, the backbone is redefined for cycles in either direction, regardless of the direction of failure. Note that for the current implementation of the limit state material model, the backbone after failure is assumed to be symmetric about the origin. This assumption is valid for columns with approximately equal flexural strengths in positive and negative bending. For columns with different flexural strengths in positive and negative bending, the backbone should be redefined such that the peak shear strength in each direction does not exceed the flexural strength in the respective direction; however, the current implementation will still be appropriate for most ground motions owing to the concentration of damage that frequently occurs in the direction of initial shear failure.

After failure is detected, the response follows the gray hysteretic curves shown in Fig. 5. Additional lateral demands will result in strength degradation of the shear spring and an increase in the shear deformations, accompanied by unloading of the beam-column element, and therefore, a slight reduction in the flexural deformations. Experimental results suggest that the shear deformations increase significantly after shear failure but do not conclusively show whether the flexural deformations increase or decrease (Sezen 2002).

Experimental studies have shown that axial failure tends to occur when the shear strength degrades to approximately zero (Nakamura and Yoshimura 2002). Hence, K_{deg} can be estimated using the calculated drift at axial failure as illustrated in Fig. 6. When shear failure is detected, based on the intersection of the total response and the shear limit curve, the degrading slope for the total response, K^t_{deg}, can be estimated as follows:

$$[2] \qquad K^t_{deg} = \frac{V_u}{(\Delta_a - \Delta_s)}$$

where V_u is the ultimate shear capacity of the column, Δ_s is the calculated displacement at shear failure, and Δ_a is the calculated displacement at axial failure for the axial load at the time of shear failure, P_s. (Note that since the column axial load can change during the analysis, Δ_s is not necessarily equal to the displacement at which axial failure is eventually detected.) Since the shear spring and beam-column element are in series, the total flexibility is equal to the sum of the flexibilities of the shear spring and the beam-column element. Hence, K_{deg} can be determined as follows:

$$[3] \qquad K_{deg} = \left(\frac{1}{K^t_{deg}} - \frac{1}{K_{unload}}\right)^{-1}$$

Note that K_{unload} must be provided as an input parameter for the limit state material model. To investigate the influ-

Fig. 5. Shear spring in series model using limit state uniaxial material model.

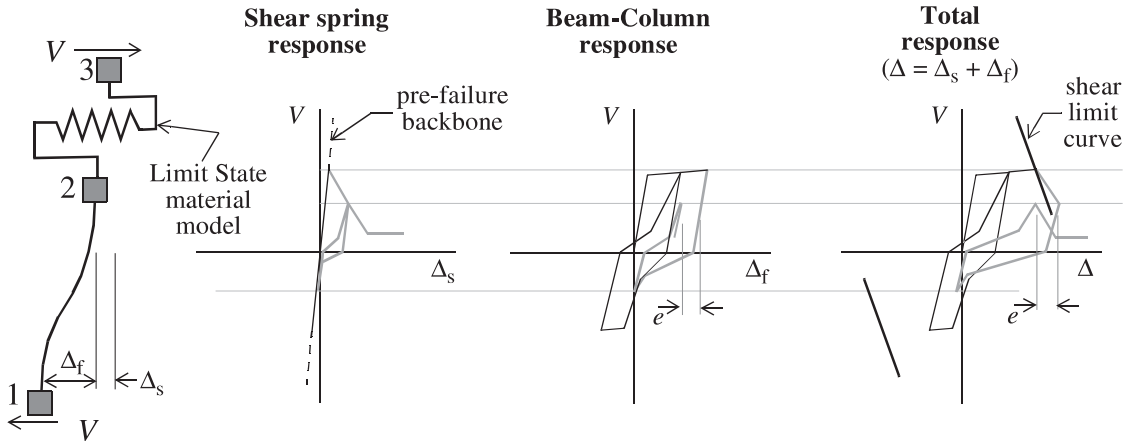

Fig. 6. Determination of degrading slope, K_{deg}.

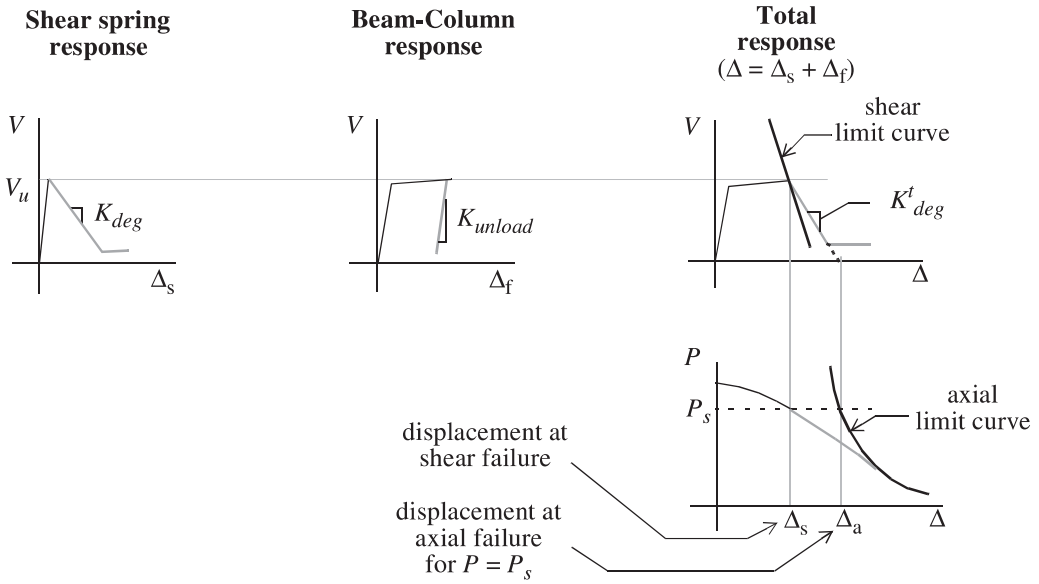

ence of different rates of shear strength degradation on the behaviour of the structural system, the material model also allows the analyst the option of specifying K_{deg} directly prior to running the analysis.

If the shear spring unloads and reloads before reaching F_{res}, as shown in Fig. 5, then a weakness of the series model becomes apparent. When the shear strength begins degrading again after reloading, the flexural displacements will be less than they were when unloading of the shear spring began (as noted by displacement e in Fig. 5). This discrepancy will result in the peak of the total response hysteresis occurring at a displacement e from the point where unloading began. Experimental results suggest that the peak should occur at a displacement close to where the unloading began. The magnitude of the offset e is dependent on the pinching characteristics modelled by the beam-column element. Considering other approximations used in the series model (for example, a linear degrading response), the offset e does not significantly detract from the effectiveness of the relatively simple series model.

The beam-column element response must have a positive slope when shear failure is detected; without a positive slope there is not a unique solution for an increase in the total displacement. Figure 7 illustrates the response of the column model for monotonically increasing total displacements. In Case 1, the beam-column response has a positive slope at shear failure, while for Case 2, a negative slope at shear failure is considered. The softening force-displacement relation for the shear spring requires that an increase in the total displacement after shear failure be accompanied by a decrease in the applied shear. For Case 1, the beam-column is forced unload to achieve the required reduction in shear. The reduction in Δ_f requires an increase in Δ_s to achieve the desired increase in the total displacement; hence, only one solution is possible. In contrast, for Case 2, the beam-column element can either unload or continue softening to achieve the required reduction in shear. This leads to three possible solutions for an increase in the total displacements: the shear spring can soften while the beam-column unloads (***b*** + ***A***), the shear spring can unload while the beam-column softens (***a*** + ***B***), or both the shear spring and the beam-column can soften (***b*** + ***B***). While all three solutions satisfy equilibrium, only the (***b*** + ***A***) solution exhibits the expected localization of damage in the shear spring. Crisfield and Wills (1988)

Fig. 7. Comparison of response given positive and negative strain hardening slopes at shear failure.

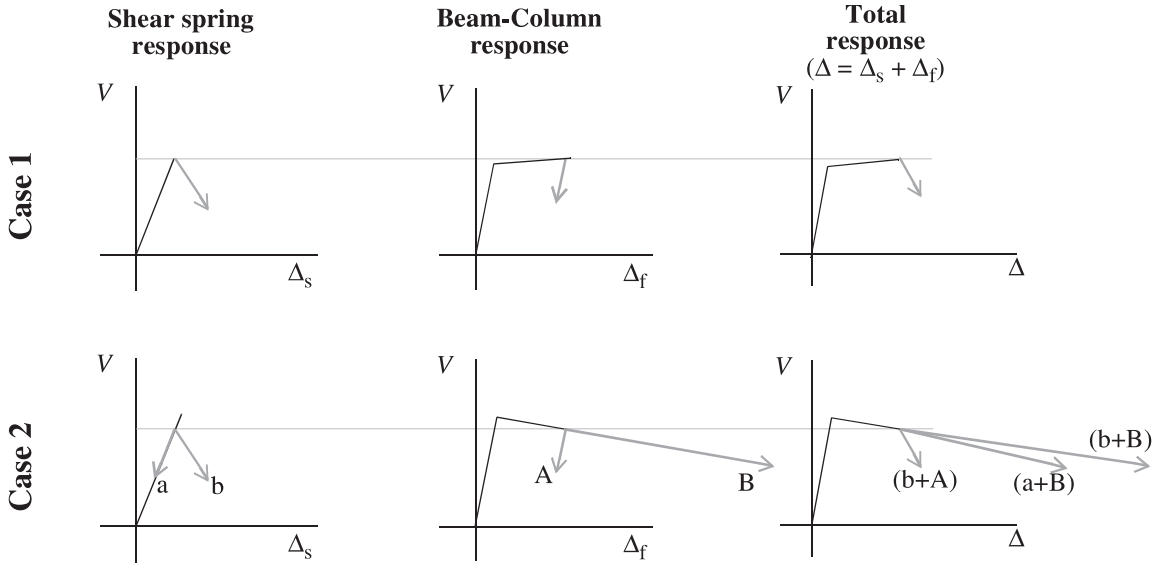

have shown that the equilibrium state upon which the solution will converge depends on the step size and the selected iterative technique. To avoid numerical convergence problems and ensure a localization of damage in the shear spring, it is recommended that the beam-column response always maintain a positive slope.

Modelling column axial failures

The limit state uniaxial material model can also be used to model axial failure where the limit curve is defined by an axial capacity model for shear-damaged columns (Elwood and Moehle 2003). The axial capacity model assumes that shear failure has already occurred and that axial failure results from sliding along a critical inclined shear crack. The model described here, and illustrated in Fig. 8, assumes that shear failure is modelled by a shear spring in series, similar to the model described above. After any analysis, postprocessing should be used to confirm that shear failure was detected prior to axial failure.

The axial capacity model by Elwood and Moehle (2003) suggests that the drift at axial failure, $(\Delta/L)_{axial}$, is inversely proportional to the axial load supported by the column and directly proportional to the amount of transverse reinforcement

$$[4] \qquad \left(\frac{\Delta}{L}\right)_{axial} = \frac{4}{100}\,\frac{1+(\tan\theta)^2}{\tan\theta + P(s/A_{st}f_{yt}d_c\tan\theta)}$$

where d_c is the depth of the column core from center line to center line of the ties, s is the spacing of the transverse reinforcement, A_{st} and f_{yt} are the area and yield strength of the transverse reinforcement, P is the axial load on the column, and θ is the critical crack angle from the horizontal (assumed to be 65°). As shown in Fig. 8, the axial failure limit curve for a given column, as defined by the Elwood and Moehle model, can be represented on a plot of axial load versus total lateral drift.

If the beam-column element includes the axial flexibility of the column, the pre-failure backbone for the axial spring should be defined by a steep straight line to ensure the spring does not add any axial flexibility to the model. If, on the other hand, the beam-column element is considered axially rigid, then the slope of the pre-failure backbone for the axial spring can be set equal to the initial axial stiffness of the column. After axial failure, the backbone will be redefined to include the degrading slope, K_{deg}, and the residual strength, P_{res}. Since the axial failure model only describes compression failure, the backbone is redefined only for compressive axial loads (shown as positive in Fig. 8).

Shear–axial coupling should be included in any model in which the behaviour after the onset of axial failure is of interest. Although very few experimental data have been collected after the onset of axial failure, shake table tests by Elwood and Moehle (2003) and large-scale pseudo-static tests by Lynn (2001) and Sezen (2002) suggest that an increase in lateral shear deformations may lead to an increase in axial deformations and a loss of axial load. Based on this general observation, the coupling model illustrated in Fig. 9 has been developed to approximate the shear–axial coupling after axial failure. The response after axial failure is shown as a gray line in Fig. 9. For any increase in lateral displacement after axial failure is detected, the P–Δ_{horz} relationship is assumed to follow the axial limit curve defined by the Elwood and Moehle model. As the earthquake imposes lateral deformations on the damaged column beyond the point of axial failure, the P–Δ_{horz} relationship will result in a loss of axial load, which will in turn lead to an increase in axial deformations owing to the P–Δ_{vert} relationship defined by the post-failure backbone of the axial spring. When the P–Δ_{horz} response is on the limit curve, the stiffness of the axial spring is set to K_{deg} to ensure the spring does not unload elastically. When the earthquake reverses the direction of motion of the structure, it is assumed that the critical shear failure crack will partially close and sliding along the crack will be arrested, resulting in temporary support of the axial load; however, since the column has sustained significant damage, the axial stiffness of the column can be assumed to be less than the elastic axial stiffness. To account for this behaviour when the P–Δ_{horz} response leaves the axial limit curve, the backbone of the axial spring is redefined such that

Fig. 8. Axial spring in series model.

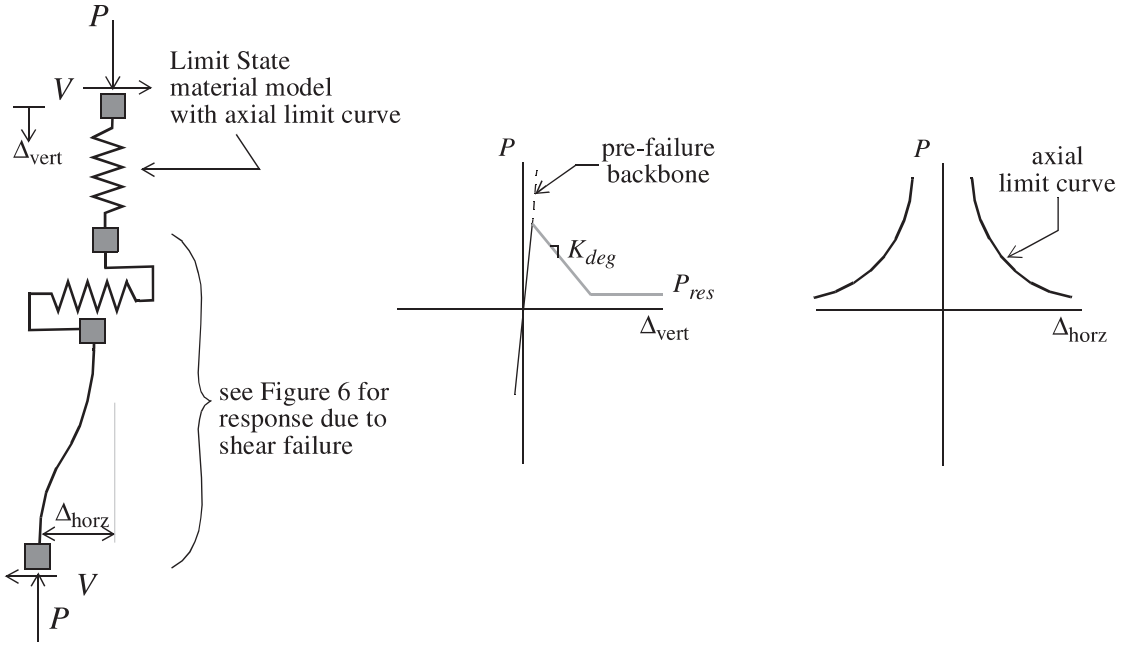

the stiffness of the spring is equal to α times the elastic axial stiffness of the column, K_e, temporarily stopping the decay along the P–Δ_{vert} backbone. Sliding along the critical shear failure plane, and hence, decay along the P–Δ_{vert} backbone, will resume if the P–Δ_{horz} response hits the limit curve again.

The softening factor α applied to the axial spring stiffness was selected to approximately represent the damage to the column core. The softening factor should be less than unity; however, further testing beyond the point of axial failure is required to provide further guidance on the selection of α. Note, if the α = 1.0 is selected, numerical convergence is frequently not achieved when the P–Δ_{horz} response moves off the axial limit curve owing to the sudden change in stiffness.

Figure 10 provides a closer look at how the material model response is forced to follow the axial limit curve after failure. Recall that exceedance of the limit curve is checked only after each converged load step to avoid "flip-flopping" between the pre- and post-failure states within a single load step. For each converged step beyond the limit surface there exists an unbalance force, P_{loss}, required to return the material model to the limit curve at the same deformation. As shown in Fig. 10, the axial load lost after each converged step beyond the limit curve is the sum of P_{loss} and axial load lost because of softening of the damaged column, P_{soft}. The total, $P_{loss} + P_{soft}$, is equal to the gravity load that must be redistributed to neighboring elements within one time step.

The differential lengthening of columns because of flexural cracking will result in coupling between Δ_{horz} and Δ_{vert} not shown in Fig. 9. For clarity, the response illustrated here assumes there is no coupling except on the axial limit curve, resulting in the horizontal and vertical lines seen on the P–Δ_{horz} and the V–Δ_{vert} plots, respectively, and the stationary points marked by solid circles on the P–Δ_{vert} plot.

Comparison of analytical model with experimental results

In this section, the response of the column model, incorporating limit state material models for shear and axial load failure, is compared with results from shake table tests by Elwood and Moehle (2003). These tests were selected for comparison because they provide data on the response of reinforced concrete columns *after* the onset of axial failure. To the author's knowledge, such data are unavailable elsewhere.

The shake table test specimens were composed of three columns fixed at their base and interconnected by a beam at the upper level (Fig. 11). The center column had wide spacing of transverse reinforcement, making it vulnerable to shear failure and subsequent axial load failure during testing. Two nominally identical test specimens were constructed and tested. The first specimen supported a mass of 300 kN, producing a center column axial load of 128 kN ($0.10f_c'A_g$). The second specimen also supported a mass of 300 kN, but pneumatic jacks were added to increase the axial load on the center column to 303 kN ($0.24f_c'A_g$). Table 1 summarizes the critical properties of the frame specimens illustrated in Fig. 11. Both specimens were subjected to one horizontal component from a scaled ground motion recorded at Viña del Mar during the 1985 Chile earthquake. Further details of the test setup and the analyses described below can be found in Elwood and Moehle (2003).

All three columns were modelled using nonlinear fiber beam-column elements (Souza 2000). Linear rotational springs were connected to each end of the beam-column elements to account for bar slip deformations. To model the shear and axial load failures of the center column, shear and axial springs were attached in series with the center column element as shown in Fig. 8. Equations [1] and [4] were used to define the limit curves for the shear and axial springs, respectively. The initial slope for the shear spring (that is, the

Fig. 9. Shear–axial coupling after axial failure for the model shown in Fig. 8.

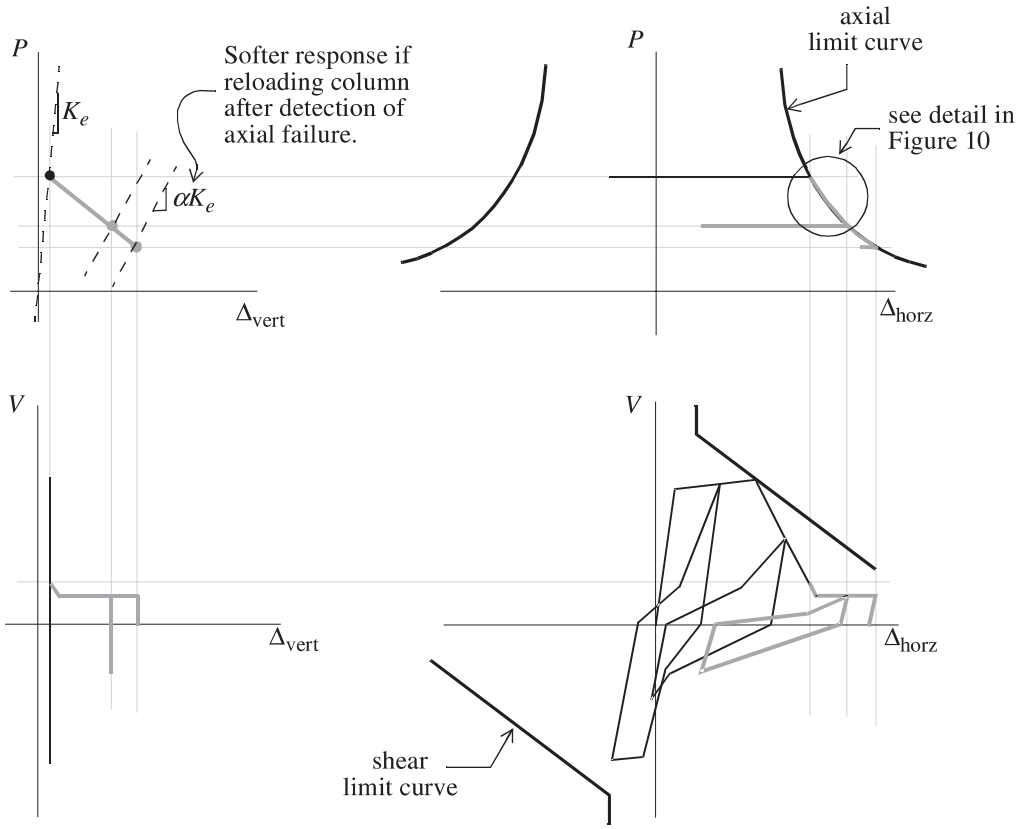

Fig. 10. Detail of axial load loss from Fig. 9.

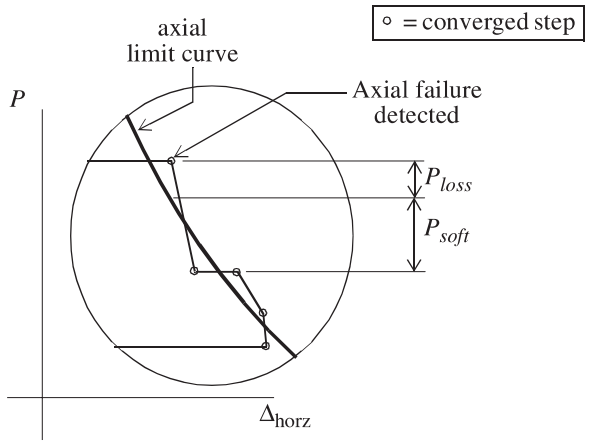

slope of the pre-failure backbone from Fig. 5) was chosen based on the shear stiffness of the uncracked column. As shown in Fig. 6, the degrading slope for the shear spring after shear failure is detected (K_{deg} from Fig. 6) was determined based on achieving the calculated drift at axial failure (per eq. [4]) once the shear strength has degraded to zero. The initial slope for the axial spring (that is, the slope of the pre-failure backbone from Fig. 8) was selected as 100 times stiffer than the axial stiffness of the column to ensure no additional axial flexibility was introduced into the model. The degrading slope of the axial spring (K_{deg} from Fig. 8) was selected as –16 kN/mm, based on a linear approximation to test data from Specimen 2. Further testing beyond the initiation of axial failure is needed to provide guidance on the selection of reasonable values for the degrading slope after axial failure. For reloading after axial failure, the softening factor α was selected to be 0.01. The beam and footings were modelled as linear-elastic.

As discussed above, for a column using the limit state failure model to define shear failure, computational issues require that the flexural response always maintains a positive slope prior to shear failure. Although the concrete for the center column could be considered unconfined owing to the wide spacing of the transverse reinforcement, to avoid a negative slope in the flexural response, the selected concrete material model for the fiber beam-column element did not allow for strength degradation after reaching the unconfined concrete compressive strength of 24 MPa. The reinforcing steel material model for the center column used a strain-hardening modulus of $0.015E_s$ (where E_s = 200 000 MPa), approximately twice that observed in the coupon tests, to ensure the *P*–Delta effects did not result in a negative slope in the flexural response. Since strength degradation after shear failure, modelled by the shear spring, governed the strength degrading behaviour of the center column, the altered concrete and steel material models did not significantly impact the calculated column response.

Static cyclic analyses were performed by applying the recorded displacement of the beam during the shake table tests to the node at the top of the center column. Such analyses are similar to those performed to validate analytical models using static test data (Pincheira et al. 1999). The results

Fig. 11. Shake table test specimens (units in millimeters).

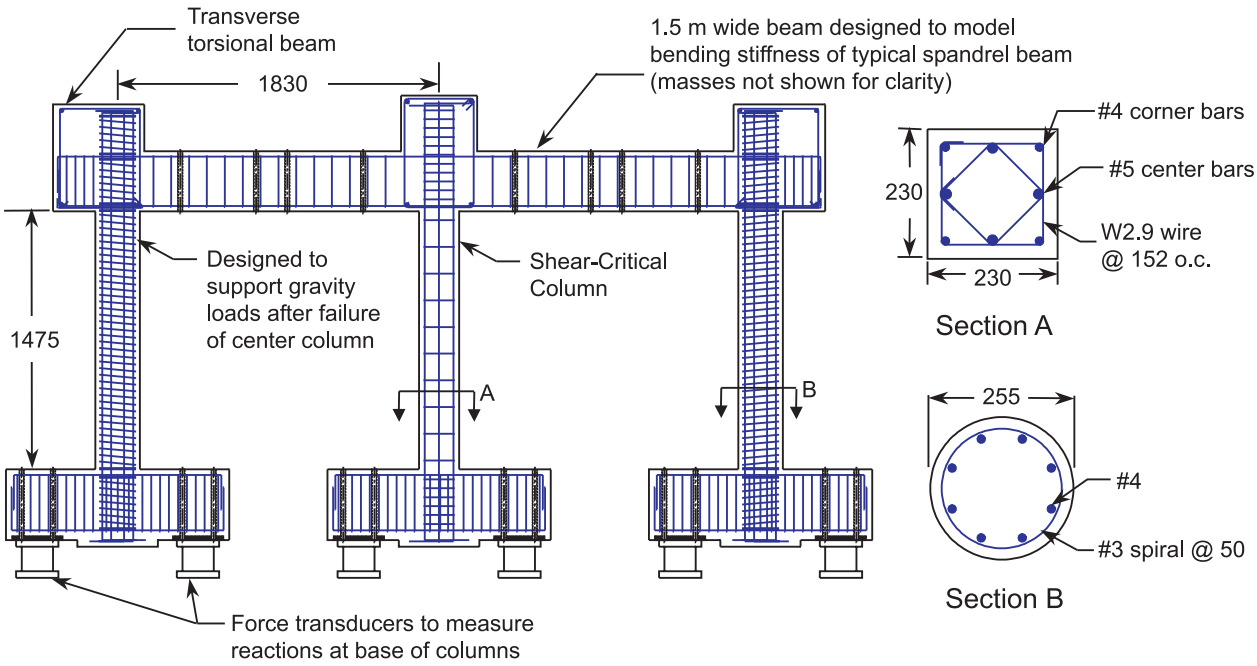

Table 1. Properties for shake table test specimens (Elwood and Moehle 2003).

f_c' (columns and beam, Specimen 1)	24.5 MPa
f_c' (columns and beam, Specimen 2)	23.9 MPa
f_y (center column longitudinal bars)	479 MPa
f_y (outside column longitudinal bars)	424 MPa
f_y (center column transverse bars)	718 MPa
Mass	300 kN
Center column axial load (Specimen 1)	128 kN
Center column axial load (Specimen 2)	303 kN
Longitudinal reinforcement ratio, ρ_l (center column)	2.5%
Longitudinal reinforcement ratio, ρ_l (outside columns)	2.0%
Longitudinal reinforcement ratio, ρ_h (center column)	0.18%

demonstrate the capability of the analytical model to reproduce the hysteretic behaviour observed during the test. Dynamic analyses, conducted with the same model, have also shown close agreement with the experimental data, although the specimen drifts tend to be underestimated. Results of the dynamic analyses can be found elsewhere (Elwood and Moehle 2003).

Shear response

Figure 12 compares the results from the static cyclic analysis with the measured shear hysteretic response for the center columns of both specimens. The analytical model adequately represents the measured response in terms of the initial and degraded column stiffness. Prior to shear failure, stiffness degradation results from the hysteretic behaviour of the concrete and steel models used to define the fiber element sections and the flexural response of the fiber element. After shear failure, the shear deformations modelled by the shear spring dominate the response of the analytical model (Fig. 13). The pinched hysteretic response of the shear spring material model provides the additional stiffness degradation observed after shear failure.

For Specimen 1, the analytical model detects that shear strength degradation begins during a negative displacement cycle at a drift ratio of –2.5%, while for Specimen 2, shear strength degradation is first detected during a positive displacement cycle at a drift ratio of 2.1%. This response is consistent with the observed behaviour for both specimens.

The bottom plots in Fig. 12 indicate that the measured shear strength degradation did not occur as rapidly as indicated by the analytical results. In particular, the measured shears for both specimens beyond a drift ratio of 4% for the large positive displacement cycles at 25 s are as much as twice that estimated by the analysis. Regardless of overestimating the rate of shear strength degradation, the model adequately represents the near-complete loss of shear strength after 28 s for Specimen 1 and 25 s for Specimen 2.

In Fig. 13, the response of the analytical model from 15 to 17.5 s is decomposed into the shear and flexural (including bar slip) deformation components. While the flexural deformations estimated by the model are similar for the two specimens, the estimated shear deformations for Specimen 2 are considerably greater than those for Specimen 1. The larger shear deformations result in the greater loss of shear strength for Specimen 2 during the cycles shown in Fig. 13. The earlier influence of shear deformations and loss of shear strength for Specimen 2 is one of the fundamental differences between the observed response of the two specimens.

Axial response

Only the center column of Specimen 2 experienced axial failure during testing, and hence the comparison of the axial response will be limited to this component. The vertical dis-

Fig. 12. Center column shear hysteretic response using static cyclic analysis.

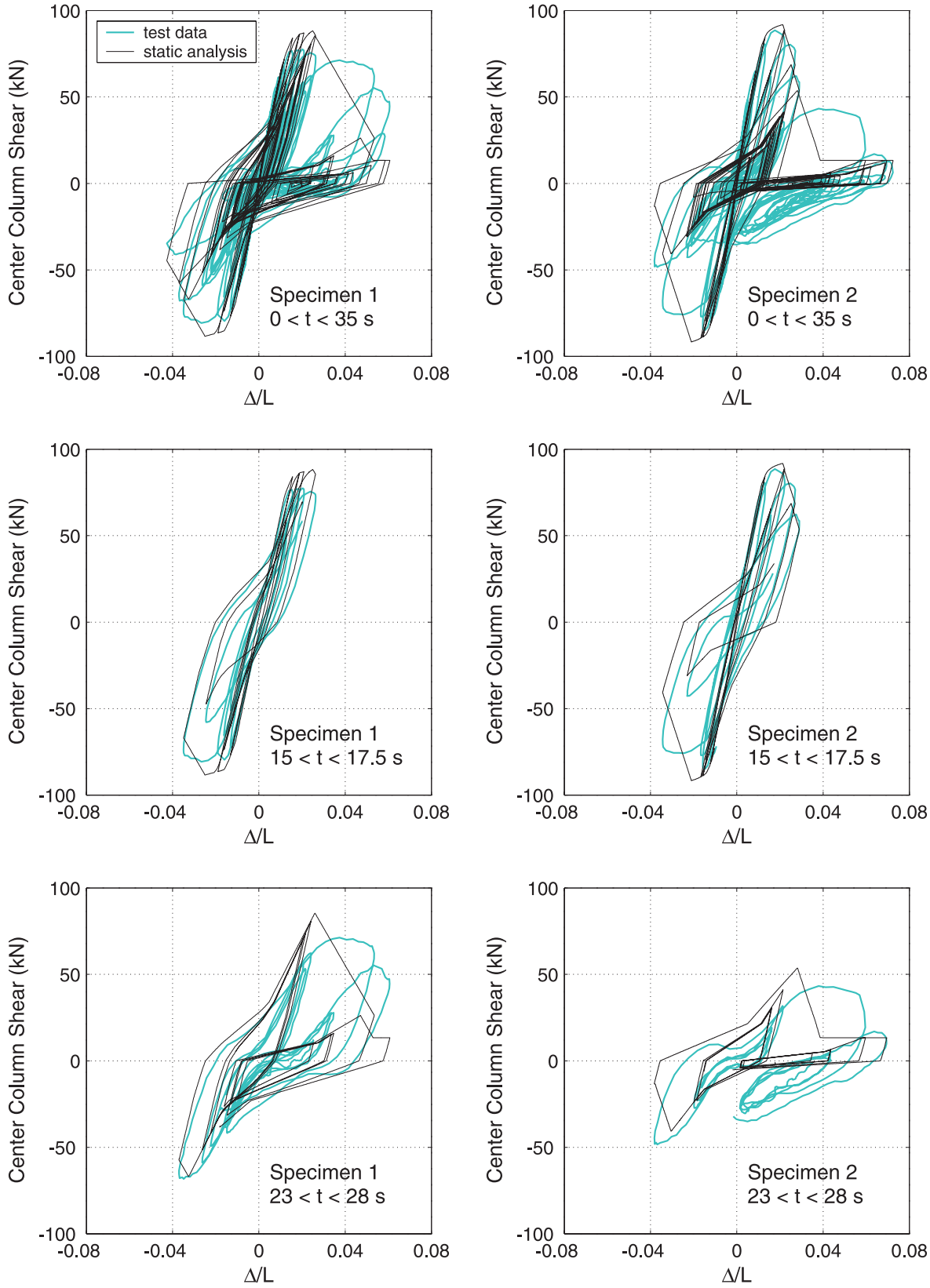

placements and axial load response for the center column are shown in Figs. 14 through 16. Owing to flexural cracking, the center column lengthens with increasing lateral displacement prior to shear failure. After shear failure, but prior to axial failure, the influence of the lateral displacements on the calculated vertical response diminishes as the shear de-

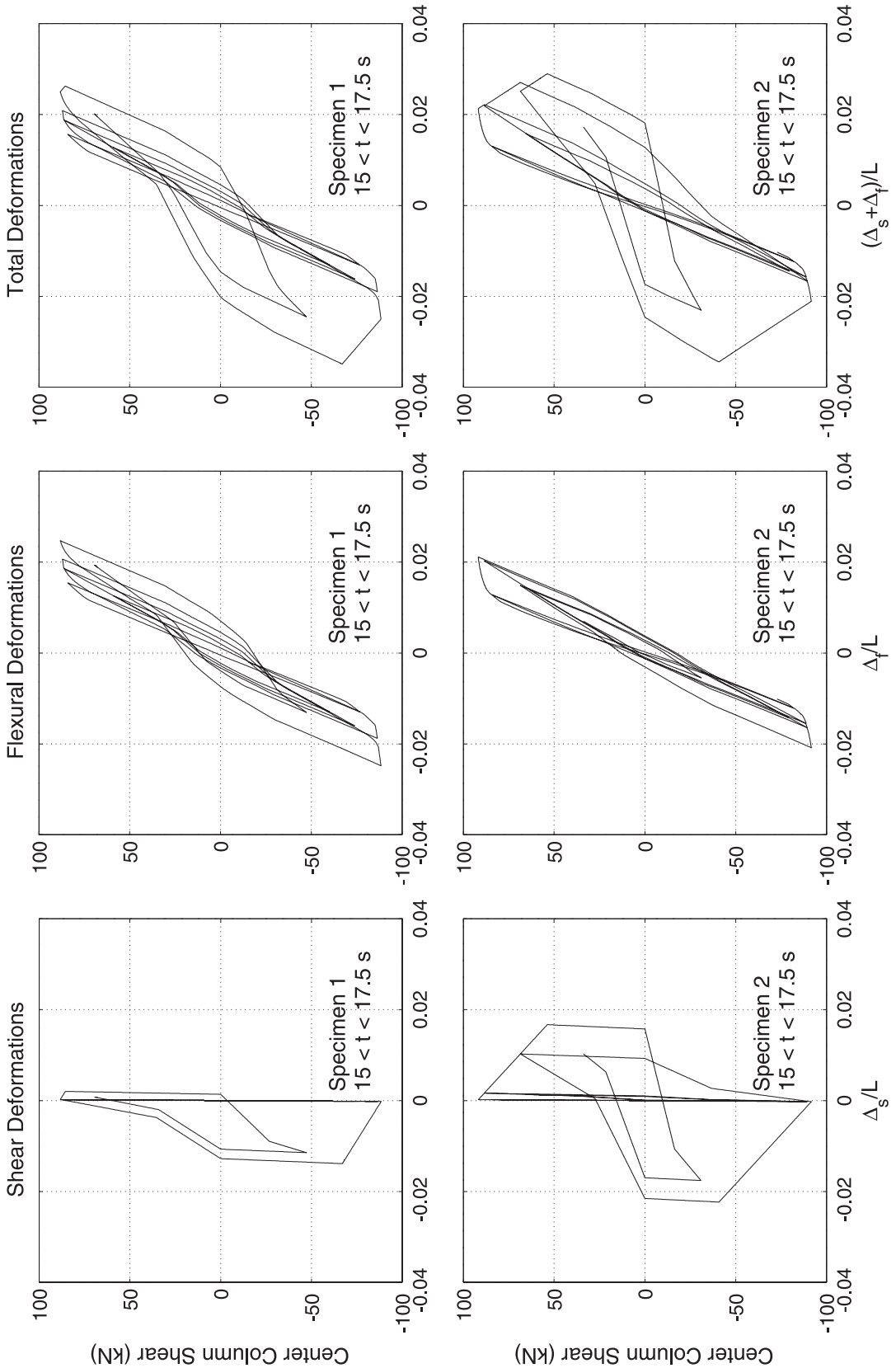

Fig. 13. Shear and flexural deformations for the center column model.

Fig. 14. Coupling of horizontal and vertical displacements at the Specimen 2 center column.

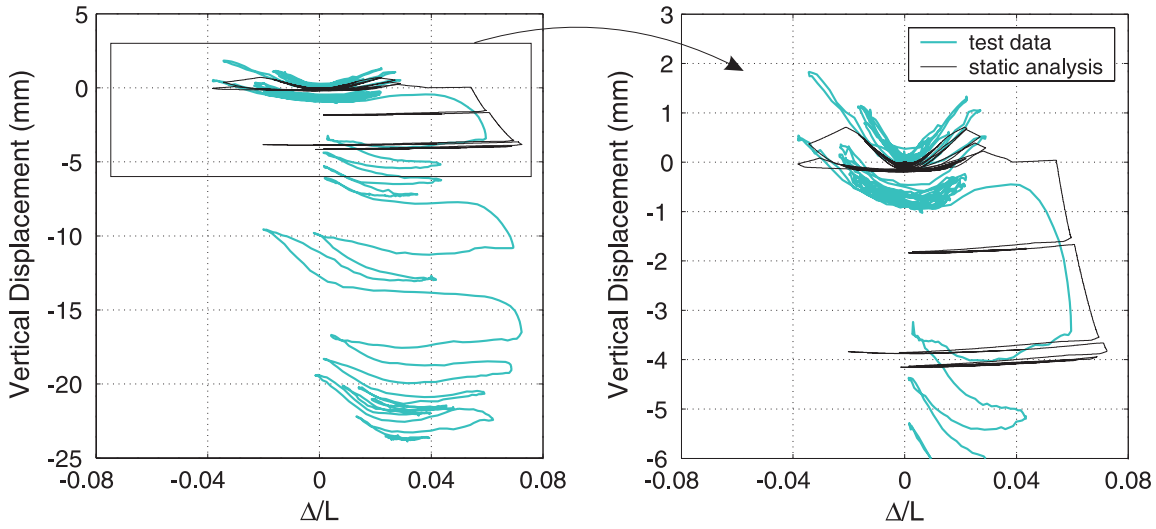

mand on the center column drops. The analytical model does not capture the 0.5 mm of downward vertical displacement accompanying shear failure (at 17 s) as seen in the test data shown in the right-hand plot of Fig. 14.

After axial failure is detected, the vertical displacements at the center column increase rapidly in the downward direction. As shown in Fig. 15, the downward vertical displacements given by the analytical model increase only while the calculated response follows the axial limit curve. While capturing some of the general characteristics of the measured axial load-vertical displacement response for the center column (left hand plot of Fig. 15) and correctly determining the timing of the first increase in downward vertical displacements (bottom plot of Fig. 16), the analytical model underestimates the increase in vertical displacements, in part due to the position of the axial limit curve. The influence of the position of the axial limit curve is investigated in more detail in Elwood and Moehle (2003).

Figure 15 shows that the axial load in the center column decreases with increasing lateral displacements owing to the difference in the vertical displacements at the center and outside columns and the accompanying bending of the beam. Since the slight downward movement of the beam at shear failure of the center column (at 17 s) is not captured by the analytical model, the accompanying 31 kN drop in the center column axial load is also not observed in the calculated results. Once the calculated results intersect the axial failure limit curve, according to the shear–axial coupling model shown in Fig. 9, the axial load in the center column is forced to follow the limit curve until the direction of motion reverses and the column begins to pick up load again. The analytical results indicate a minimum axial load of 107 kN, compared with a measured minimum axial load of 44 kN. While underestimating the total axial load lost, the analytical model reproduces many of the critical characteristics of the center column axial load response history, as shown in Fig. 16.

Effect of variability on the limit state failure model

The accuracy of any analysis using the limit state failure model described in this paper is limited by the accuracy of the capacity models used to define the limit curves and the ability of the hysteretic rules to represent the behaviour after failure. While further study is required to improve estimates of the limit curves and the degrading behaviour after shear and axial failure, significant variability in the estimates is expected to remain because of the extent of damage expected at the point of shear and axial failure. Limited experimental studies on the response of reinforced concrete columns after shear failure, and particularly after axial failure, make reliable assessment of the variability difficult.

Owing to the significant change in the response of the structure once a limit curve is reached, the limit state failure model is particularly sensitive to any variability in the limit curves. For example, if a conservative estimate of the axial capacity limit curve is used and failure is detected in a column, then the additional gravity load redistributed to other columns may lead to their failure and a progressive collapse of the structure. If, on the other hand, a limit curve representing the mean axial capacity is used, then failure of the first column may not be detected and no collapse would ensue. The sensitivity of the system response to the variability of the limit curves must be accounted for directly when evaluating the results from any analysis using the limit state failure model.

Research by other investigators may enable the use of the limit state failure model in a probabilistic assessment of the structural response. Work by Gardoni et al. (2002) can be used to construct probabilistic capacity models based on the deterministic limit curves presented here. Work by Haukaas (2003) will allow the probabilistic capacity models to be included in a finite element analysis using the limit state failure model and OpenSees, resulting in the assessment of the probability of collapse. Such probabilistic modelling is beyond the scope of the current study, but should be considered in future research.

Summary and conclusions

A relatively simple uniaxial material model has been developed to model the failure of reinforced concrete compo-

Fig. 15. Variation of Specimen 2 center column axial load with vertical displacement and drift ratio.

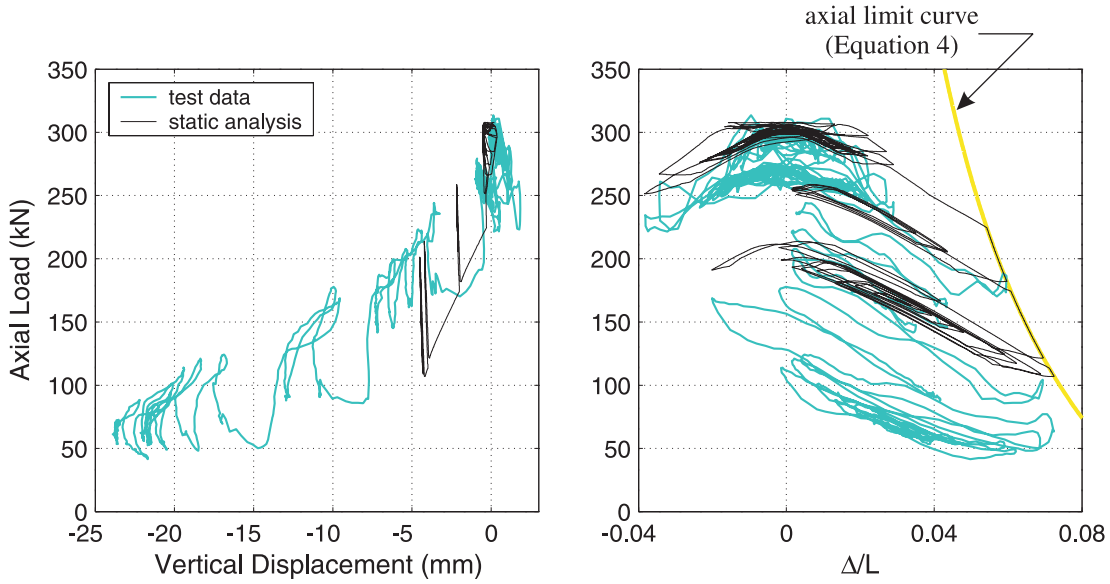

Fig. 16. Axial load and vertical displacement response histories for Specimen 2 center column.

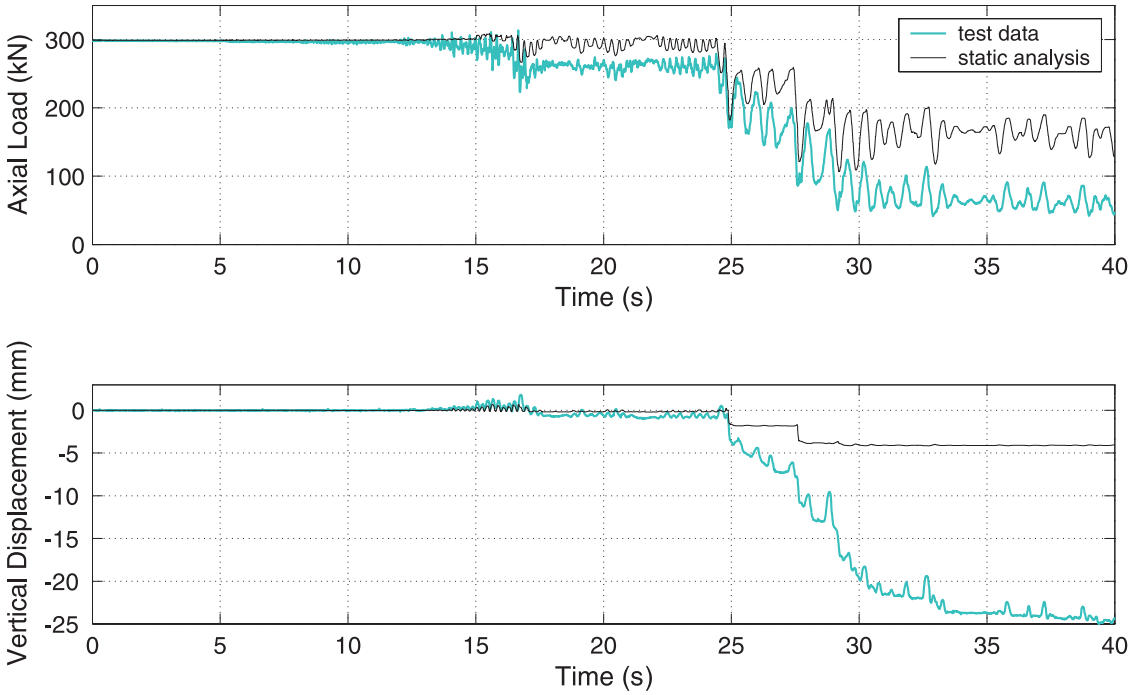

nents. The material model detects the point of failure based on the response of an associated beam-column element intersecting a predefined limit state failure surface. The limit state failure surface can change shape or move during an analysis based on the response of the element it describes (for example, the limit state failure surface describing shear failure of a column may be dependent on the axial load on the column, and thus, will move as the axial load on the column changes during the analysis). After failure of the reinforced concrete component is detected, the strength of the uniaxial material model degrades with increasing deformations. When the uniaxial material model is connected in series with the associated beam-column element, the strength degradation of the material model will limit the load carried by the beam-column element and effectively model the strength degradation of the reinforced concrete component.

In this paper, the uniaxial material model has been applied to the shear failure and axial failure of existing reinforced concrete columns. This material model enables shear failure of a reinforced concrete column to be defined in terms of multiple variables that may change during the course of an analysis, including, shear force, lateral drift, and axial load.

After shear failure is detected the material model can estimate the rate of shear strength degradation based on an estimate of the drift at axial failure. The material model can also capture axial failure of the column, accounting for changes in the axial load and lateral drift during the analysis. Shear–axial coupling was incorporated in the material model to approximate the response of a column after the onset of axial failure. The coupling model was based on very limited experimental data and, as such, may not be representative of the behaviour of columns with different details and subjected to different ground motions. More experimental data after the onset of axial failure is required to improve the shear–axial coupling model.

Comparison of the analytical model with shake table test data indicated that, while simplifying the response after shear and axial failure, the relatively simple material model adequately captured many of the critical characteristics of the specimen response. The analyses accurately determined the timing of the shear and axial load failures and captured the increase in shear deformations after shear failure and the variation in the center column axial load after axial failure. The total loss of axial load and the vertical shortening of the center column were underestimated by the analyses. By incorporating such a column model in a building frame analysis it is possible to account for the influence of shear and axial failures of individual columns on the response of the building system.

Acknowledgements

The advice of Professor Jack Moehle and Dr. Frank McKenna significantly contributed to the development of the limit state failure model presented in this paper. The work was supported in part by the Pacific Earthquake Engineering Research Center through the Earthquake Engineering Research Centers Program of the National Science Foundation under Award number EEC-9701568. This support is gratefully acknowledged.

References

Aschheim, M., and Moehle, J.P. 1992. Shear strength and deformability of RC bridge columns subjected to inelastic displacements. University of California, Berkeley. Report UCB/EERC 92/04.

Crisfield, M.A., and Wills, J. 1988. Solution strategies and softening materials. Computer Methods in Applied Mechanics and Engineering, **66**: 267–289.

Elwood, K.J., and Moehle, J.P. 2003. Shake table tests and analytical studies on the gravity load collapse of reinforced concrete frames. Pacific Earthquake Engineering Research Center, University of California, Berkeley, Calif. PEER Report 2003/01.

Elwood, K.J., and Moehle, J.P. 2005. Drift capacity of reinforced concrete columns with light transverse reinforcement. Earthquake Spectra, **21**. In press.

Gardoni, P., Der Kiureghian, A., and Mosalam, K.M. 2002. Probabilistic capacity models and fragility estimates for reinforced concrete columns based on experimental observations. Journal of Engineering Mechanics, **128**(10): 1024–1038.

Haukaas, T. 2003. Finite element reliability and sensitivity analysis of hysteretic degrading structures. Ph.D. thesis, Department of Civil and Environmental Engineering, University of California, Berkeley, Calif.

Kang, T.H.-K., and Wallace, J.W. 2004. Shake table tests of reinforced concrete flat plate frames and post-tensioned flat plate frames. Proceedings of the13th World Conference on Earthquake Engineering, Vancouver, B.C., 1–6 August 2004. Mira Digital Publishing, St. Louis, Mo. Paper No. 1119.

Lynn, A.C. 2001. Seismic evaluation of existing reinforced concrete building columns. Ph.D. thesis, Department of Civil and Environmental Engineering, University of California, Berkeley, Calif.

McKenna, F., Fenves, G.L., and Scott, M.H. 2004. *OpenSees*: Open system for earthquake engineering simulation. Pacific Earthquake Engineering Research Center, University of California, Berkeley, Calif. Available from [accessed 1 September 2004].

Nakamura, T., and Yoshimura, M. 2002. Gravity load collapse of reinforced concrete columns with brittle failure modes. Journal of Asian Architecture and Building Engineering, **1**(1): 21–27.

Pincheira, J.A., Dotiwala, F.S., and D'Souza, J.T. 1999. Seismic analysis of older reinforced concrete columns. Earthquake Spectra, **15**(2): 245–272.

Priestley, M.J.N., Verma, R., and Xiao, Y. 1994. Seismic shear strength of reinforced concrete columns. Journal of Structural Engineering, **120**(8): 2310–2329.

Ricles, J.M., Yang, Y.-S., and Priestley, M.J.N. 1998. Modelling nonductile R/C columns for seismic analysis of bridges. Journal of Structural Engineering, **124**(4): 415–425.

Sezen, H. 2002. Seismic response and modeling of reinforced concrete building columns. Ph.D. thesis, Department of Civil and Environmental Engineering, University of California, Berkeley, Calif.

Shirai, N., Moriizumi, K., and Terasawa, K. 2001. Cyclic analysis of reinforced concrete columns: macro-element approach. Modeling of Inelastic Behaviour of RC Structures under Seismic Load, American Society of Civil Engineers, Reston, Va. pp. 435–453.

Souza, R.M.d. 2000. Force-based finite element for large displacement inelastic analysis of frames. Ph.D. thesis, Department of Civil and Environmental Engineering, University of California, Berkeley, Calif.

Watanabe, F., and Ichinose, T. 1992. Strength and ductility of RC members subjected to combined bending and shear. *In* Concrete shear in earthquake. *Edited by* T.T.C. Hsu and S.T. Mau. Elsevier Applied Science, New York. pp. 429–438.